Effects of interparticle interactions in magnetic Fe/Si_3N_4 granular systems

F. Jiménez-Villacorta, J. Sánchez-Marcos, E. Céspedes, M. García-Hernández, and C. Prieto
Instituto de Ciencia de Materiales de Madrid, Consejo Superior de Investigaciones Científicas, Cantoblanco, 28049 Madrid, Spain
(Received 8 March 2010; revised manuscript received 26 July 2010; published 8 October 2010)

An experimental evidence of the progressive modification in the magnetic behavior of granular Fe/Si_3N_4 samples due to interaction effects between particles is reported. Microstructural features and local structure were determined by x-ray absorption spectroscopy and transmission electron microscopy to select granular samples with predetermined cluster size. Fe/Si_3N_4 systems have been characterized by ac- and dc-magnetization measurements to study the gradual evolution of magnetic properties of granular systems, where three different behaviors have been observed. As-deposited samples with Fe thickness layers of 2.5 nm, present a modified superparamagnetic behavior, due to very weak interactions between very small Fe clusters separated by a nonmagnetic FeN phase. An evolution of the average blocking temperature at intermediate fields ($T_B \sim H^{3/2}$) is observed, similar to noninteracting systems, but first signatures of a frozen spin state at low temperatures appear. Annealed samples exhibit a noticeable modification from the multilayer character to a random three-dimensional organization of Fe clusters embedded in a Si_3N_4 matrix. After annealing, samples with initial Fe layer thickness of 0.7 nm provide iron cluster in the range of 1.3 nm and exhibit a superspin-glass state, with a de Almeida-Thouless evolution of the energy barriers ($T_B \sim H^{2/3}$) that is explained in terms of increasing interparticle interactions. Moreover, annealed samples, with initial layer thickness of 1.3 nm, supply iron cluster of near 3 nm that present stronger interactions and yield a superferromagnetic state, likely provided by residual ultrasmall particles between the blocked clusters.

DOI: 10.1103/PhysRevB.82.134413 PACS number(s): 75.75.Cd

I. INTRODUCTION

Granular magnetic materials formed by metal-ceramic systems are of great interest due to their intrinsic physical properties, such as large tunnel magnetoresistance and enhanced coercivity.[1–4] Intense research on this type of systems is being extraordinary fuelled by the refinement of preparation and synthesis methods and the development of characterization techniques. The observation of new phenomena exhibited by such materials at the nanoscale, such as increasing anisotropy,[5,6] rise up of ferromagnetic (FM) signal due to the modification of electronic configuration[7,8] or glassy state[9] may arise from finite-size effects, interplay between surface and core atoms or surface spin frustration. In the latter case, spin-glasslike features, attributed to the dominant role of surface spins, have been deduced from a de Almeida-Thouless[10] (AT) dependence of their magnetothermal behavior.[11,12]

Competing interactions between magnetic particles can also modify the magnetic features of nanosystem.[13,14] For instance, interparticle interactions in concentrated nanoparticle systems can affect the height and distribution of the energy barriers. Interactions between particles may imply an increase in the average blocking temperature in both ac- and dc-magnetization measurements.[15,16] It has been stated that a transition from superparamagnetic (SPM) to spin-glasslike behaviors, or even to superferromagnetism (SFM), can be due to interactions between superspins (magnetic moments of the ferromagnetic nanoparticles).[17,18] As an open question, one of the main challenges is to elucidate the contributions of dipolar, exchange and tunneling exchange interactions, as well as to distinguish the contributions to the effective barrier distribution of dipolar interactions and surface spin frustration.

An increase in the concentration of magnetic particles yields to a transition from a SPM state to a disordered collective behavior, named superspin-glass (SSG) state.[19] In the last years, effects of interactions on the magnetic relaxation in systems presenting such superspin-glass state have been studied using ac-susceptibility measurements.[13,20] Recently, some examples have shown the effects of such SSG state also in dc-magnetothermal curves. Sahoo *et al.*[18] show an AT dependence of the blocking temperatures of discontinuous $[Co_{80}Fe_{20}(0.9\ nm)/Al_2O_3(3\ nm)]$ multilayers, observed by zero-field-cooling-field-cooling (ZFC-FC) magnetothermal curves at very weak fields ($H<50$ Oe), with a destruction of the AT behavior at intermediate fields, proposing a crossover into a chiral glass regime. Similar results also at low fields ($H<60$ Oe) have been observed in interacting γ-Fe_2O_3 nanoparticles.[21] They observed as well a small dip-and-plateau structure in FC curves below the irreversibility temperature in the more concentrated sample (volume fraction $=35\%$), whereas the diluted sample (0.01%), which presents a noninteracting superparamagnetic particle behavior, shows a continuous decrease in the FC magnetization while increasing the temperature. Suzuki *et al.*[17] roughly approximate the evolution of the ZFC peak temperature to an AT dependence line in interacting Fe_3O_4 nanoparticles at low and intermediate fields, with a H-T phase diagram following $H \sim H_0(1-T/T_f)^{1.78}$ (being constants H_0 and T_f). They also assert that the low-temperature superspin-glass behavior is experimentally characterized by observation of the flatness in FC magnetization curves below the blocking temperature. Kremenovic *et al.*[22] have found an AT transition line in the evolution of the maxima of the ZFC curves with the applied field. They observed as well an increase in the FC magnetization reaching a maximum below the irreversibility when decreasing temperature, followed by a decrease at very low temperatures. They ascribed this behavior to the presence of either interparticle dipole-dipole interaction or exchange coupling.

In this work, we report on a detailed study of the magnetic properties of interacting granular iron in the Fe-Si_3N_4 system. Granular multilayers prepared by sequential magnetron sputtering have been obtained by progressively decreasing the metal layer thickness.[23] Such discontinuous metal-insulator multilayers are found to be very useful systems to tune magnetic interactions by simply modifying the metal layer thickness. Silicon nitride is a promising material to be used as an insulator matrix in metal/ceramic granular systems and multilayers, and it has been proposed for applications in electronic devices due to its transport and optical properties and chemical inertness at high temperatures.[24–27] However, to our knowledge, not much has been reported about Fe/Si_3N_4 systems to obtain multilayered and granular magnetic materials. Structural characterization, prior to the analysis of the magnetic properties, has been achieved by using x-ray and transmission electron microscopy (TEM) techniques. X-ray reflectometry (XRR) has given information about the microstructural features of the layers, such as thickness and roughness and TEM has been used to determine the granular character of samples. X-ray absorption spectroscopy measurements have been performed to determine the iron oxidation state as well as the local order around Fe atoms. ac- and dc-magnetization measurements were performed to observe the modifications of the spin dynamics and the energy barriers due to magnetic interparticle interactions.

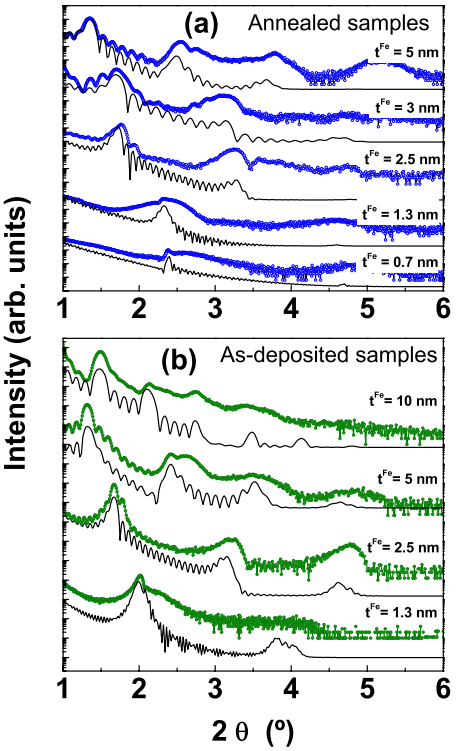

FIG. 1. (Color online) X-ray reflectivity of selected Fe/Si_3N_4 multilayers. (a) Annealed samples and (b) as-deposited samples.

II. EXPERIMENTAL

Multilayered films with general formula $[Fe(t^{Fe})/Si_3N_4(3\ nm)]_n$ were prepared by sequential magnetron sputtering. Further details of the deposition process can be found elsewhere.[23,28] Several sets of samples, with constant silicon nitride layer thickness and variable iron thickness (t^{Fe} from 5 to 0.7 nm) were prepared in order to study the formation of iron clusters. The number of bilayers (n) was increased to preserve a constant amount of Fe along the series. In previous works, an intermediate FeN phase was detected at the interface regions between the Fe clusters and the Si_3N_4 matrix in as prepared multilayers.[23] In order to minimize the presence of this minority nitride phase,[29] a selected set of samples have been subsequently annealed in vacuum ($\sim 10^{-6}$ mbar) at 700 °C for 2 h. Samples are labeled by ASD- and ANN- taking into account its "as-deposited" or "annealed" characteristic followed by the corresponding t^{Fe} value in tenths of nanometers.

XRR was achieved in a D8-Brucker AXS diffractometer with an x-ray energy of the Cu K_α. Microstructural features, such as layer thickness and average roughness were obtained by fitting the experimental data with the XREAL software.[30] Fe K-edge x-ray absorption spectra were achieved in the fluorescence yield mode at the Spanish CRG beamline (SpLine-BM25) of the ESRF. The incoming beam was monitored by a N_2-filled ionization chamber, and the Fe K_α fluorescence line was detected using a one element Si(Li) detector (from e2V Scientific Instruments).

Electron microscopy studies were undertaken using a 200 kV JEOL2000FX. Films were prepared following a cross-sectional configuration for TEM by using the standard procedure: mechanical grinding, dimpling (using a GATAN656) and argon ion milling (Fischione 1010) in a liquid-nitrogen-cooled holder with an acceleration voltage of 3–5 kV and an incidence angle of 8°. The high-resolution analysis provided precise information of the microstructural features of our samples.

dc magnetic measurements with the applied field parallel to the film plane were performed in a superconducting quantum interference device magnetometer (MPMS-5, from Quantum Design). Magnetization loops at different temperatures were recorded after applying a cooling field of 20 kOe. Magnetothermal ZFC-FC curves were measured as a function of the increasing temperature at different probing fields. Likewise, ac magnetization was measured at different frequencies, ranging from 100 to 9000 Hz, in a PPMS-9T (from Quantum Design) susceptometer.

III. RESULTS

Prior to the magnetic study of granular Fe/Si_3N_4 system, a microstructural characterization is presented. In order to test the multilayered structure of the films and to determine the layer thickness, samples have been characterized by XRR. Figure 1 shows the obtained data from a selection of samples and their best-fit simulations. The actual thicknesses of Fe layers (t^{Fe}) are given at the figure (they were obtained after assuming constant values for Si_3N_4 layers). In spite of the small differences observed after annealing in the reflectivity, no variations in bilayer thickness were detected. Additionally, XRR gives an average roughness near 1 nm for all

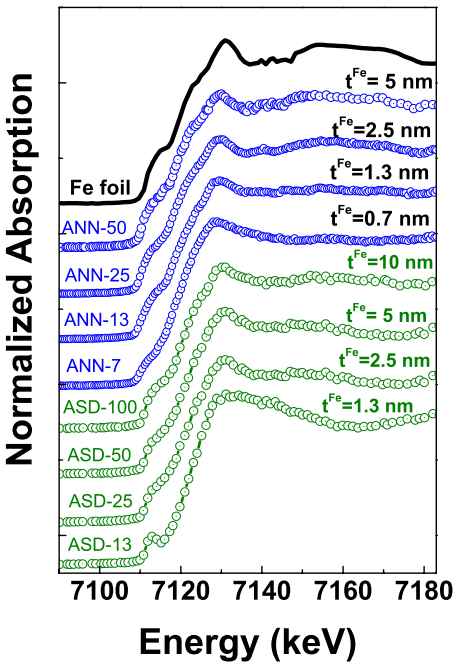

FIG. 2. (Color online) XANES spectra of annealed (ANN- label) and as-deposited (ASD- label) series of Fe/Si_3N_4 multilayers, a Fe foil spectrum is given for reference.

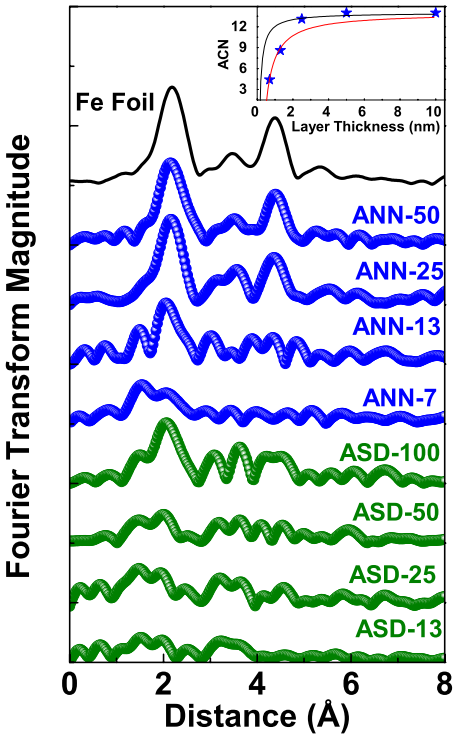

FIG. 3. (Color online) Fourier transforms of EXAFS signals corresponding to the annealed and as-deposited Fe/Si_3N_4 series. Inset shows the average coordination number (estimated by the coordination number reduction) vs the iron layer thickness. Lines are obtained according Eq. (1) with $\alpha=15$ (upper curve) and $\alpha=45$ (lower curve).

studied samples. It should be remarked that, though the simulations were successful in reproducing the shape of experimental data for multilayers with large t^{Fe}, no suitable simulation to reproduce conveniently the two samples with smaller t^{Fe} has been found. This fact suggests that samples with t^{Fe} values on the order of 1 nm are candidates to show a granular behavior. To sum up, taking into account the estimated values of average Fe layer thickness and roughness, and supported by the remarkable change in reflectivity along the annealed multilayer series having an intensity decrease and a broadening of superstructure peaks for the thinner t^{Fe} samples, a transition from continuous to discontinuous Fe layers for samples with $t^{Fe}<2.5$ nm should be taken into account.

Figure 2 shows the x-ray absorption near-edge structure (XANES) of the multilayers. Data corresponding to the analog *as-deposited* samples have been taken form Ref. 23 and added in the figure for comparison. Results show that the *annealed* samples with large Fe layers reproduce the XANES features of the metallic Fe. However, as the Fe layer decreases, subtle differences appear in all the spectra. Small changes in the edge structures, evolving through the formation of a pre-edge feature can be observed. Also, a slight increase in intensity in the dip at around 7140 eV and a subtle reduction in the broad shoulder centered at 7180 eV is observed as the Fe layer thickness decreases. Since such evolution appears for the samples with the thinnest Fe layers, it can be interpreted as an enhanced contribution of the interface Fe atoms, which may present an alternative local environment arrangement. In the as-deposited samples, the presence of a local geometry around Fe different from that of the metallic phase is already apparent. This has been attributed to an enhanced contribution of a FeN phase present at the interface regions.[23]

Extended x-ray-absorption fine structure (EXAFS) analysis confirms these results. Fourier transforms shown in Fig. 3(a) exhibit a remarkable reduction in the intensity of the peak associated to metal Fe-Fe distances (≈ 2 Å) for samples with $t^{Fe}\leq 1.3$ nm. This is consistent with the loss of nearest neighbors of Fe atoms at the surface of small particles. Furthermore, a peak associated to Fe-N coordination in tetrahedral geometry appears at smaller distances (≈ 1.5 Å).[31] Data corresponding to the as-deposited samples are also given; the comparison with its corresponding annealed sample is representative of the annealing effect that provides an increase in the metallic phase and the practical disappearance of the Fe-N phase for samples with initial iron layer thickness higher than 1.3 nm, being a physical system that permits to study the magnetic behavior of particles as a function of its size and its interparticle distance.

Table I gives the evolution of the structural parameters of annealed samples obtained by the EXAFS analysis. These results are consistent with the XANES spectra, though the large amount of the pure metallic component in the thin layers is still the main contribution. Finally, it should be noted that the reduction in the Fe-Fe coordination together with an enhanced Fe-N contribution is more visible in the as-deposited sample.

Additionally, we have used a model which relates the average coordination number (ACN) obtained by the EXAFS analysis with the bulk coordination number (CN^{bulk}) the microstructure (layer thickness and roughness) estimated by XRR,[28]

TABLE I. Summary of EXAFS obtained parameters: distance (R), number of neighbors (N), and Debye-Waller factor (σ^2). Particle size (d^{Fe}) estimated from the EXAFS obtained average coordination number reduction and from the TEM images analysis. [Results of as-deposited Fe(**2.5** nm)/Si_3N_4(3 nm) sample are taken from Ref. 23].

Fe(t^{Fe})/Si_3N_4(3 nm) sample	Pair	R (Å)	N	σ^2 ($\times 10^{-3}$ Å^2)	d^{Fe} EXAFS (nm)	d^{Fe} TEM (nm)
Fe foil	Fe-Fe	2.48	8.0	4.9		
	Fe-Fe	2.86	6.0	7.1		
Annealed Fe(**5** nm)/Si_3N_4(3 nm)	Fe-Fe	2.48 ± 0.01	8.0 ± 0.1	5.5		
	Fe-Fe	2.85 ± 0.01	6.0 ± 0.1	7.9		
Annealed Fe(**2.5** nm)/Si_3N_4(3 nm)	Fe-Fe	2.48 ± 0.01	7.7 ± 0.2	5.5		
	Fe-Fe	2.85 ± 0.01	5.4 ± 0.2	9.9		
Annealed Fe(**1.3** nm)/Si_3N_4(3 nm)	Fe-Fe	2.47 ± 0.01	5.4 ± 0.5	5.5	2	3.3
	Fe-Fe	2.86 ± 0.01	3.2 ± 0.5	9.9		
	Fe-N	1.85 ± 0.02	2.7 ± 0.5	4.2		
Annealed Fe(**0.7** nm)/Si_3N_4(3 nm)	Fe-Fe	2.46 ± 0.02	3.3 ± 0.5	5.5	1.2	1.3
	Fe-Fe	2.80 ± 0.04	1.4 ± 0.5	9.9		
	Fe-N	1.93 ± 0.04	3.4 ± 0.5	4.2		
As-deposited Fe(**2.5** nm)/Si_3N_4(3 nm)	Fe-Fe	2.44 ± 0.02	2.0 ± 0.5	6.4	0.9	
	Fe-N	1.89 ± 0.04	3.5 ± 0.5	4.2		

$$\mathrm{ACN} = \mathrm{CN}^{bulk}\left[1 - \frac{\alpha R}{2t}\right], \tag{1}$$

where R is the first neighbor distance, t is the layer thickness, and α is a parameter which takes into account the layer roughness. This model introduces an "effective" thickness, t/α, smaller than the nominal one, in such a manner that when t/α becomes on the order of the atomic distances the continuous layer evolves to a discontinuous one. For annealed samples, a plot of ACN values vs layer thickness [Fig. 3(b)] defines two differentiated behaviors: $t^{Fe} \geq 2.5$ nm samples are fitted with $\alpha = 14$ and $t^{Fe} \leq 1.3$ nm samples with $\alpha = 45$. This is a clear hint that two microstructural regimes are observed, yielding the formation of Fe clusters for small enough Fe layers.

In the cluster regime, an estimation of the average grain size can be obtained. A direct relationship between the average number of neighbors and the mean size of the particles can be obtained by using an adequate particle shape model.[32,33] By assuming spherical clusters, the estimation gives Fe particles with average diameters of $d^{Fe} \approx 2$ nm and around $d^{Fe} \approx 1.2$ nm for ANN-13 and ANN-7 samples, respectively. It should be noted that an average size of $d^{Fe} \approx 0.9$ nm was reported for Fe particles in ASD-25 sample.[23]

Figure 4 depicts high-resolution transmission electron micrographs of the ANN-13 and ANN-7 annealed films. From such micrographs, it is clear that films present characteristics of a granular system. After considering a statistics based in more than 400 particles, size distributions are also given. ANN-13 exhibits a remarkably broad size distribution, it has been fitted by a Gauss function [Fig. 4(b)], which yields an average particle diameter of $d^{Fe} = 3.3$ nm with an important contribution of smaller particles. ANN-7 sample presents clearly smaller particle dimensions with a narrower particle distribution [Fig. 4(d)], the Gauss fit leads to an average particle sized of $d^{Fe} = 1.3$ nm. Both values are in good agreement with those obtained with EXAFS analysis.

Figure 5 shows the magnetization loops at 10 K of as-deposited samples, with nominal Fe layer thickness of 5, 2.5, and 1.3 nm (ASD-50, ASD-25, and ASD-13, respectively) and annealed samples with the three smallest layer thickness $t^{Fe} = 2.5$, 1.3, and 0.7 nm (ANN-25, ASD-13, and ASD-7). As-deposited samples present a noticeable evolution from the observed FM behavior in ASD-50 to SPM in ASD-25 and paramagnetic in ASD-13. This transition is accompanied by a drastic reduction in the magnetization signal between the ASD-50 and ASD-25 samples. Furthermore, ASD-13 sample scarcely presents a visible magnetization signal explained by its observed strong iron nitridation. This obtained behavior is in agreement with the transition from continuous iron layers to granular magnetic systems when the average iron layer thickness reduces down to $t^{Fe} = 2.5$ nm.

ASD-25 presents a strong SPM component, which does not reach saturation at high fields [insets of Fig. 5(a)]. An estimation of the metallic Fe cluster size, performed in the EXAFS analysis, give an average particle diameter of around $d^{Fe} \approx 0.9$ nm, much lower than the nominal Fe layer thickness.[23] A successful explanation for such behaviors is that these *as-prepared* samples present a remarkable presence of a FeN nonmagnetic phase. This FeN phase contributes to reduce the magnetization values and to separate physically the iron clusters, preventing interaction between them and, thus, leading to the strong granular SPM character of the ASD-25 sample. Having this sample such SPM behavior, it can be used as representative of very weakly interacting magnetic particle systems in order to study the effects in the magnetic features provided by increasing interparticle interactions.

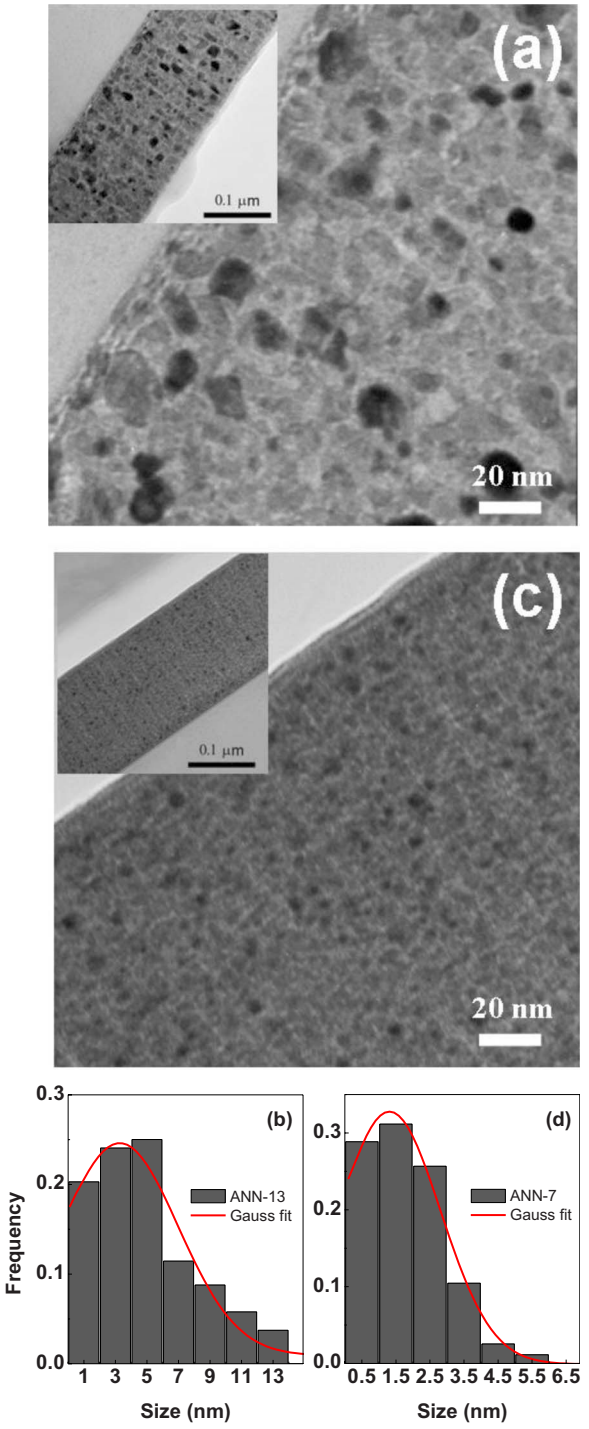

FIG. 4. (Color online) Transmission electron microscope cross-section images and particle size distribution of two characteristic annealed samples. [(a) and (b)] Annealed Fe(1.3 nm)/Si_3N_4(3 nm) sample (ANN-13). [(c) and (d)] Fe(0.7 nm)/Si_3N_4(3 nm) sample (ANN-7).

In the annealed set, as the Fe layer thickness decreases, a noticeable decrease in remanence, as well as, of magnetization with temperature can be observed [as it is seen in the 300 K loops of inset in Fig. 5(b)]. ANN-13 and ANN-7 samples do not reach saturation at room temperature and loops present rounded shape. All these facts suggest a granular behavior, in agreement with the nonpercolated granular morphology observed by TEM. However, whereas ANN-13 exhibits coercivity at room temperature, ANN-7 presents SPM behavior at room temperature without coercivity or remanence. Along the series, the contribution of a SPM component progressively increases by decreasing the Fe thickness, ANN-13 sample shows a small but visible contribution of a SPM phase. Furthermore, the reduction in size and the increase in interparticle distance, in ANN-7 sample, leads to an almost typical SPM behavior at room temperature, with coercivity and remanence tending to zero and no saturation at high fields.

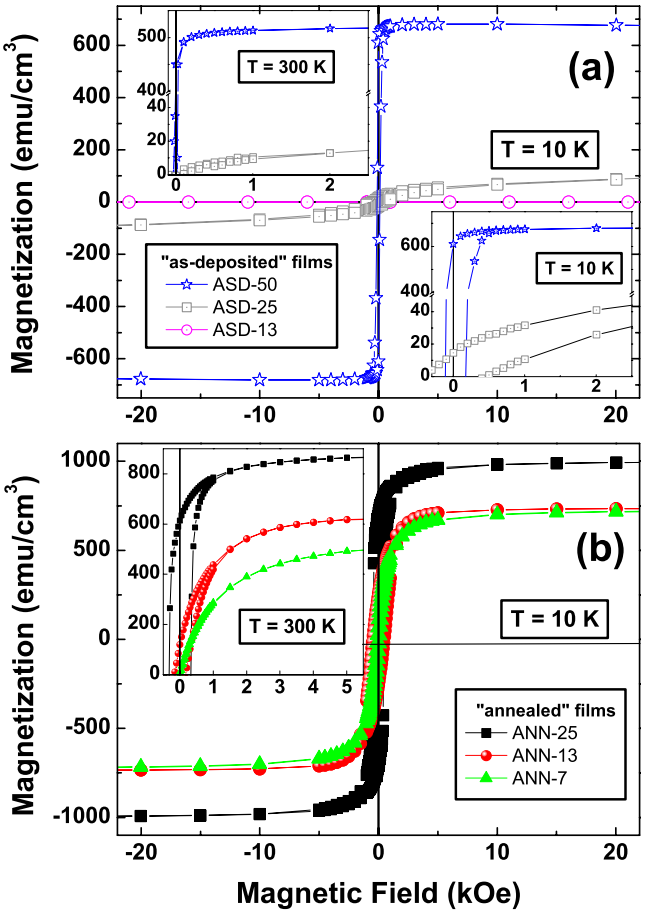

FIG. 5. (Color online) Magnetization loops at different temperatures of the Fe/Si_3N_4 multilayers (normalization has been made to the total volume of Fe layers). (a) As-deposited samples. (b) Annealed samples. Insets show detail of the loops at $T=10$ and 300 K.

Magnetization values of ANN-13 and ANN-7 samples are significantly smaller (especially at room temperature) than the obtained for samples with thicker Fe layers. Also, as it will be discussed below, it is observed that coercivity in ANN-13 decreases more rapidly with increasing temperature than in ANN-25. Magnetic properties are in agreement with the structural characterization, which leads to conclude that the two annealed samples with the thinnest Fe layer thickness (ANN-13 and ANN-7) are below the physical percolation threshold and present a granular behavior consistent with average cluster dimensions of $d^{Fe} \approx 3$ nm and $d^{Fe} \approx 1.3$ nm, respectively.

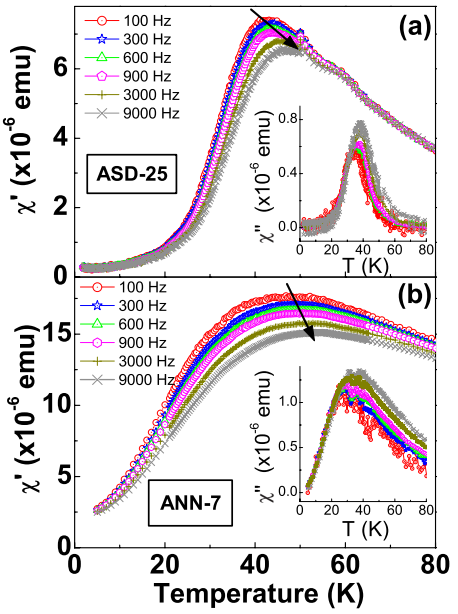

FIG. 6. (Color online) Real and imaginary parts of the ac magnetization at several frequencies: (a) as-deposited Fe(2.5 nm)/Si_3N_4(3 nm) and (b) annealed Fe(0.7 nm)/Si_3N_4(3 nm) samples.

Figure 6 shows the ac-magnetization measurements of ASD-25 and ANN-7 as representative samples of granular systems (in comparison, no appreciable signal was detected at the imaginary part of susceptibility in ANN-13). First of all, it should be noted the remarkable differences in the magnetic dynamics of these samples. A broader peak in the imaginary and real parts of susceptibility, correlated with a large distribution of energy barriers, is observed in ANN-7 sample, suggesting the effect of dipolar interactions between magnetic clusters, without neglecting the effects of a broader particle size distribution. In addition, both samples show an evolution of the maximum blocking temperature (T_{ac}^{max}) with the frequency variation. Although the estimation of T_{ac}^{max} shift may not be accurate due to broadening of the energy distribution; it is clear that ASD-25 sample shows a diminution of the T_{ac}^{max} values from 47.5 to 41 K with increasing frequency, and however, ANN-7 shows slightly weaker frequency dependence, varying from 52.5 to 47.5 K within the same frequency range. That different dependence on frequency indicates the presence of spin disorder in the later sample and is a signature of spin glass freezing at low temperatures.

Figure 7 shows ZFC-FC magnetothermal curves of ANN-13, ANN-7, and ASD-25 samples; at first glance, different behaviors are clearly observed between them. ANN-13 sample presents a ferromagnetic behavior; its FC curves show a scarce dependence on temperature and ZFC curves present up to reaching the FC magnetization values a slight and almost constant increase in magnetization with increasing temperature. Since the Si_3N_4 layers are sufficiently thick (continuous layers) and the average Fe thickness is below the intraplanar percolation threshold (t^{Fe} smaller than twice the mean roughness) that prevents also from possible two-dimensional exchange ferromagnetism, ANN-13 sample seems to be a high concentration particle system, exhibiting

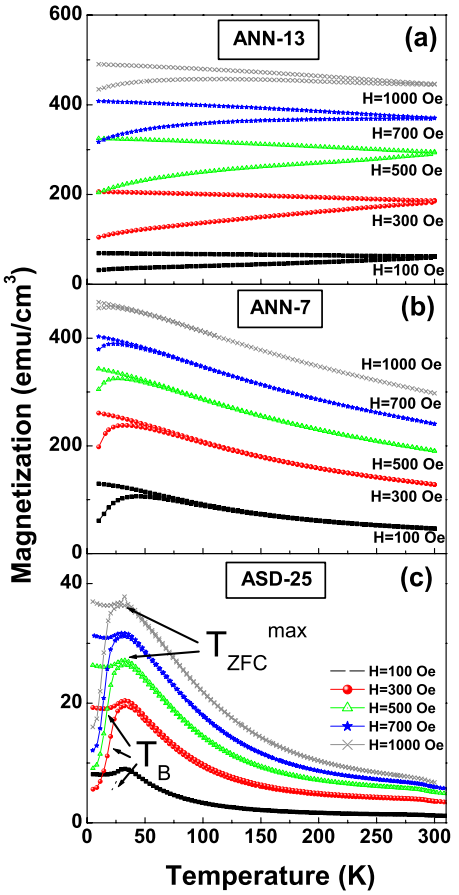

FIG. 7. (Color online) ZFC-FC curves at different intermediate fields of representative granular samples: (a) annealed Fe(1.3 nm)/Si_3N_4(3 nm), (b) annealed Fe(0.7 nm)/Si_3N_4(3 nm), and (c) as-deposited Fe(2.5 nm)/Si_3N_4(3 nm) samples.

SFM. Very similar ZFC curve shapes, as a result of strong ferromagnetic correlations between particles, have been observed in granular CoFe(1.6 nm)/Al_2O_3(3 nm) systems and ascribed to particle superferromagnetic behavior.[34] SFM has been observed for the first time by Morup *et al.*[35] in goethite nanoparticles of 10–100 nm diameter. In our case, the dense packing in ANN-13, attending to the TEM micrographs, and the strong correlations between particles, extracted from the observation of the ZFC curves, together with the rounded-shape loops and nonzero coercivity at room temperature exhibited by this sample, suggest that this high particle concentrated sample exhibits clear hints of SFM. This SFM character has been previously observed in discontinuous metal-insulator multilayers with similar metallic layer thickness in which magnetic percolation, reached without the presence of physical percolations, seems to be mediated by ultrasmall paramagnetic particles between the superspin particles.[36–38] This explanation is in agreement with the presence of an important contribution of very small particles, according to the size distribution obtained by TEM analysis. On the other hand, ANN-7 presents features characteristic of particle systems. ZFC curves show an important dependence on temperature, reaching a field-dependent maximum which resembles the overcoming of energy barriers due to thermal effects. An increase in the magnetization at room tempera-

tures with increasing fields is commonly attributed to weak interaction effects between the magnetic clusters.

Finally, ZFC-FC curves of ASD-25 shows typical features of SPM behavior. At high temperatures, the magnetic behavior is dominated by thermal fluctuations and spins are virtually independent. A Curie-Weiss dependence of the magnetothermal curves can be observed with increasing temperature. In contrast, irreversibility appears at all intermediate fields below a given critical blocking temperature, with a value that slightly decreases with increasing field. This may suggest a signal of at least small cooperative behavior.[21,39] The shape of the ZFC curve below this critical temperature resembles that of a particle blocking distribution.

IV. DISCUSSION

The granular metal-insulator systems obtained by means of a decrease in the Fe layer thickness from annealed $[\mathrm{Fe}(t^{\mathrm{Fe}})/\mathrm{Si_3N_4}(3\ \mathrm{nm})]$ multilayered films represent a suitable scenario to study the progressive evolution of magnetic properties with modification of the magnetic interparticle interactions. The gradual shrinking of the nominal Fe layer thickness may yield a reduction in the average magnetic particle size, implying an increasing separation among the metallic clusters and a subsequent decrease in the magnetic interactions between particles. For this reason, a detailed characterization of the magnetic features has been done in order to shed some light in the understanding of the effects of interactions in the magnetic properties of granular metal-insulator materials. In addition, a thorough characterization of the ASD-25 sample with a reduced average Fe particle size of $d^{\mathrm{Fe}} \approx 0.9$ nm, due to the remarkable presence of Fe in the nitride phase between Fe particles, has been introduced as representative of superparamagnetic character, typical from a very weakly interacting magnetic particle system.

Figure 8 shows the evolution of remanence (M_{R}) and coercivity (H_{C}) of three representative granular samples. ANN-13 sample ($d^{\mathrm{Fe}} \approx 3$ nm) presents larger values of magnetization and a smooth temperature dependence of M_{R}; however, the other two samples with smaller particle size show a more abrupt temperature dependence of M_{R}, being negligible at 100 K for ANN-7 sample ($d^{\mathrm{Fe}} \approx 1.3$ nm) and at 35 K for ASD-25 ($d^{\mathrm{Fe}} \approx 0.9$ nm).

Coercive field shows a similar evolution with decreasing Fe particle size. Whereas there is a sustained coercivity with increasing temperature with a monotonous slow decrease for ANN-13, an abrupt decrease in H_{C} is present in ANN-7 and ASD-25 samples. They both reach negligible values of H_{C} at 100 K and 35 K, respectively, revealing an increase in the blocking temperature attributed to increasing magnetic interactions. In ANN-13 sample, exchange interactions between particles tend to maintain its FM character when increasing the temperature. However, possible interactions between particles in ANN-7 are not strong enough to maintain remanence and coercivity as the temperature increases, giving a SPM character to this granular system at room temperature.

Interaction effects in nanoparticle systems can be tested by performing a detailed study of the magnetic response

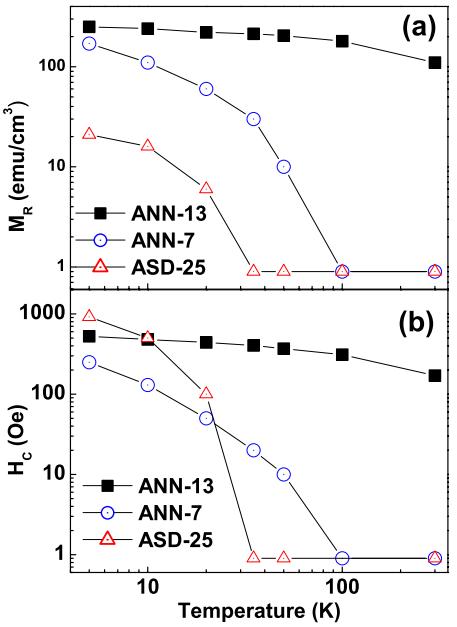

FIG. 8. (Color online) Evolution of (a) remanence and (b) coercivity with temperature of three representative granular samples. (In this logarithmic representation, the negligible values of M_{R} and H_{C} have been plotted as 1 emu/cm^3 and 1 Oe, according with the incertitude limit.)

through ac-magnetization measurements.[40] Namely, $T_{\mathrm{ac}}^{\mathrm{max}}$ in such ac measurements can be defined as the temperature for which the characteristic relaxation time is equivalent to the inverse of measuring frequency (ν). Hence, we have analyzed the frequency shift of $T_{\mathrm{ac}}^{\mathrm{max}}$ according the Neel-Arrhenius expression but the obtained characteristic relaxation time of 10^{-19} and 10^{-25} s for ASD-25 and ANN-7 samples, respectively, becomes unphysical small values. This fact leads to conclude that there exist some magnetic interactions among particles. The Vogel-Fulcher law better describes a magnetically interacting particle system,[41]

$$\tau = \tau_0 \exp[-KV/k_{\mathrm{B}}(T_{\mathrm{ac}}^{\mathrm{max}} - T_0)]. \quad (2)$$

Figure 9(a) shows the evolution of the susceptibility peak with variation in frequency to fit the evolution of $T_{\mathrm{ac}}^{\mathrm{max}}$ with Eq. (2). For ASD-25 ($d^{\mathrm{Fe}} \approx 0.9$ nm) sample fits very well the linear curve with the following parameters: $\tau_0 \approx 10^{-13}$ s that is a typical value of SPM particles, activation energy of $KV \approx 0.06$ eV and $T_0 \approx 10$ K that suggests the presence of very weak interactions between particles. Similarly, ANN-7 sample fit gives: $\tau_0 \approx 10^{-10}$ s, $KV \approx 0.026$ eV and $T_0 \approx 33$ K showing an increasing interparticle interactions respect to ASD-25.

Additionally, we have also checked the existence of spin-glass behavior in ANN-7 through a conventional critical slowing down model[42] with a power-law dependence of the characteristic time near the spin-glass transition,

$$\tau = \tau_0[T^*/(T_{\mathrm{ac}}^{\mathrm{max}} - T^*)]^{\alpha}. \quad (3)$$

In this case, fitting gives $\tau_0 \approx 10^9$ s, $T^* \approx 38$ K (and $\alpha \approx 16$), which are similar to the obtained by using the Vogel-Fulcher

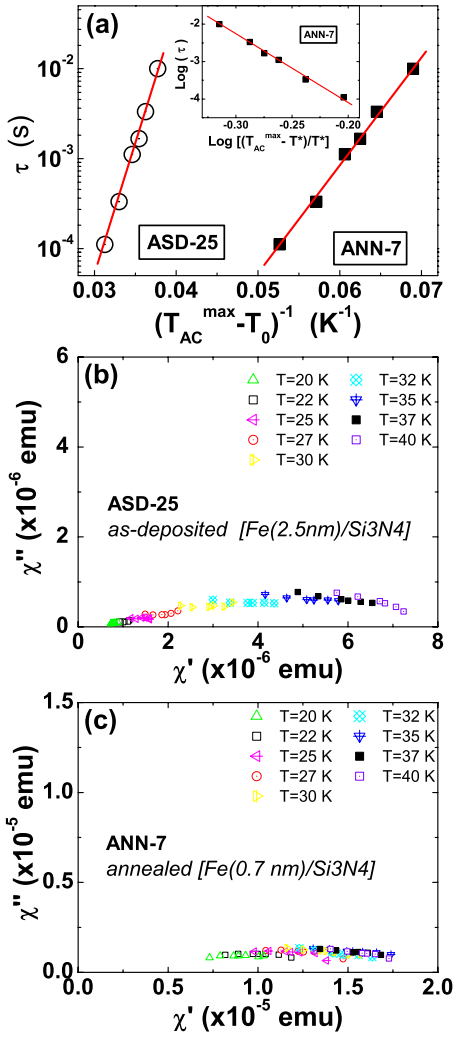

FIG. 9. (Color online) (a) Inverse of the measuring frequency vs the reciprocal of the temperature of susceptibility peak (T_{ac}^{max}) and T_0 for ASD-25 and ANN-7 samples, with T_0 values of 10 K and 33 K, respectively; inset is a log-log plot of frequency vs the reduced temperature used in Eq. (3) for ANN-7 sample with $T^*=38$ K. (b) and (c) Cole-Cole plots for ASD-25 and ANN-7 samples, respectively.

law and lets to conclude that ANN-7 has a spin-glasslike behavior.

In order to identify the dynamic behavior of the freezing-blocking process, we have estimated the values of the empirical parameter, $\Psi=[\Delta T(\upsilon)/T(\upsilon_1)\Delta \log(\upsilon)]$.[43] In ASD-25, it is found $\Psi\approx 0.07$, a value similar to those obtained for noninteracting or weakly interacting SPM particle systems. For ANN-7, values around $\Psi\approx 0.03-0.04$ are found, entering in the range of canonical spin glasses and interacting particles with glassy behavior.[15]

A final analysis of the dynamic response of such granular systems can be provided by the Cole-Cole plot.[44] Figures 9(b) and 9(c) depict the imaginary part of susceptibility vs the real one for ASD-25 and ANN-7 samples at several temperatures below T_{ac}^{max}. It should be noted that a similar representation for ANN-13 sample gives a completely flat curve because of no signal is observed at the susceptibility imaginary part. It is observed that, even if broadening occurs when temperature approximates T_{ac}^{max}, ANN-7 exhibits remarkably flattened curves for every temperature, respect to ASD-25. All these features indicate an increase in interaction between particles with a characteristic size of $d^{Fe}\approx 1.3$ nm in ANN-7 sample, respect to ASD-25, which recalls the collective behavior of SSG systems[19] and let to describe ANN-7 sample as a SSG system formed by particles of 1.3 nm.

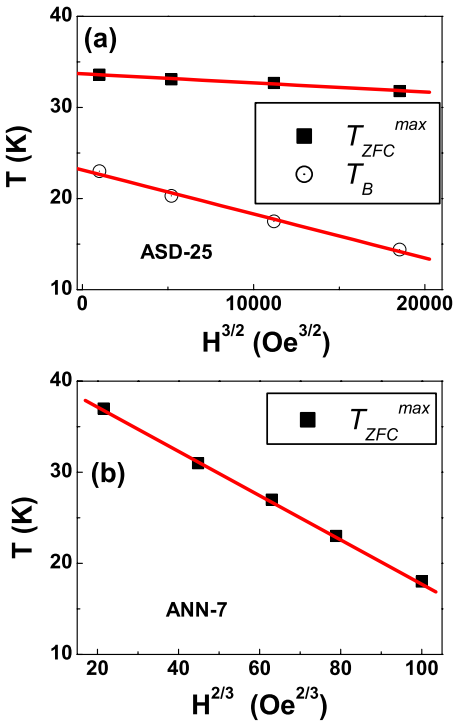

FIG. 10. (Color online) Dependence of the blocking temperature with the applied magnetic field (a) as-deposited Fe(2.5 nm)/Si_3N_4(3 nm) and (b) annealed Fe(0.7 nm)/Si_3N_4(3 nm) samples.

Interactions result in modifications of the blocking and reorientation processes of dc magnetothermal curves. We have plotted this progressive evolution in Fig. 10 of experimental values taken from data of Fig. 7. Besides the dispersion of blocking distribution, an increasing applied field yields a reduction in the average blocking temperature in a particle system, and thus in a decrease in the maximum of the ZFC curve. For noninteracting particle systems with uniaxial anisotropy a $T_B\sim H^{3/2}$ dependence was predicted by Victora,[45]

$$T_B \sim T_{B0}\left[1-\frac{H}{H_k}\right]^{3/2} \tag{4}$$

where T_{B0} is the blocking temperature at zero field, which is related to the anisotropy energy ($T_{B0}\sim KV$) and observed experimentally by Nunes *et al.*[39] in Co-SiO_2 granular films. In Fig. 10, we have plotted T_B values corresponding to ASD-25 sample obtained from the inflexion point in ZFC curves at different fields, which lets to observe that its average blocking temperature in ASD-25 clearly follows the $H^{3/2}$ evolution at intermediate fields (between 100 and 1000 Oe).

Additionally, the maxima of the ZFC curves, which set the point of the blocking temperature for the biggest particles, T_{ZFC}^{max}, seem to follow as well such $\sim H^{3/2}$ dependence in a weak way. In this case, in agreement with the ac-magnetization analysis, very weak interactions between particles can be deduced, since they follow precisely the Curie-Weiss law, with an estimated ordering energy around 10 K. Both FC and ZFC curves present an increase in the magnetization with decreasing temperature above the blocking temperature, in a thermodynamic equilibrium state. Below the blocking temperature, the ZFC curves present an evolution interpreted by a narrow distribution of particles sizes. On the other hand, the FC curves flatten at low temperatures, presenting small maxima around T_{ZFC}^{max} at intermediate field. These small peaks can be attributed to appreciable differences between the cooling rate and the heating rate during the experiments when measuring particle systems.[46]

However, ANN-7 sample presents remarkable differences respect to ASD-25. Blocking temperatures decrease as well with increasing magnetic field (H) but in this case, the evolution presents a clear AT dependence,[10]

$$T_B \sim T_{B0}\left[1 - \frac{H}{H_k}\right]^{2/3} \tag{5}$$

Figure 10(b) illustrates such evolution of T_{ZFC}^{max} with probing fields. It should be noted that in this case, evolution of the average blocking temperatures cannot be properly represented because values are in the low limit of temperature range measurements, which may be explained by the broadening of the energy barrier distribution provided by relatively broad particle size distributions and interparticle interactions. This AT line defines the onset of a transition between a frozen spin-glasslike state and the magnetic reversibility behavior. Interactions dominate the properties for small applied fields since it is expected that the applied field would dominate over the nearest-neighbor interactions as the system approaches saturation.[47]

On the other hand, such dipolar interactions impinge on the ZFC magnetothermal curves as follows: at the beginning, when the sample is being cooled down, the magnetic moments of the particles present a disordered state and are randomly oriented. As the temperature increases, the particle moments tend to orientate along the direction of the field, which increases the magnetization following a particle distribution of energy barriers. Conversely, dipolar interactions between particle moments, that are not totally oriented along the field direction, exert a weak pinning between them leading to a spin-glasslike behavior.

In previous works, it has been theoretically predicted that dipolar magnetic interactions between particles provides an AT dependence in highly concentrated particle systems.[47] On the other hand, the existence of spin-glasslike phase in particle systems, observing an $\sim H^{2/3}$ dependence, has been pointed as a result of diverging relaxation times, attributed to competing interactions between surface spins (thus, disorder showed by a spin-glass phase shell surrounding a defined magnetic core).[4,12] In this case, if the spin-glasslike state would be due only to the existence of a frozen state of spins at the surface, this behavior would be observed as well in the ASD-25 sample, which presents an interface forming Fe-N bonds.[23] However, it exhibits a canonical $T_B \sim H^{3/2}$ dependence, typical from magnetic particle systems with very weak interactions. Hence, it can be deduced that the spin-glasslike behavior in such particle system is due to simple dipolar interactions between the magnetic superspins.

Moreover, one outstanding aspect should be remarked. At intermediate fields, a plateau can be observed in the FC curves of the ASD-25 sample as it may be observed in Fig. 7(a). While increasing the applied field, the paramagnetic tail effect of very small SPM particles seems to alter the constant shape of the plateau, leading to the formation of a very smooth dip in the magnetization values at around 15–25 K. This dip-and-plateau feature is characteristic of interacting particle systems.[19,21] However, as interaction increases, such as in the case of ANN-7 sample (having an AT dependence of the energy barriers) the FC magnetization curves decreases monotonically with increasing temperature below the blocking temperatures.

It is usually assumed that a signature of the SSG phase is the temperature-independent flatness of the field-cooled susceptibility below the freezing temperature. But in cases previously reported, the plateau appears at very low fields[17,21,48] and at intermediate fields, the FC curves below T_B seem to exhibit a small but monotonic decrease with increasing temperature.[17,18,22] In ANN-7 sample (having a SSG behavior), a plateau is not observed at intermediate probing fields in the FC curve below the AT line but it appears in the SPM ASD-25 one. Hence, a general conclusion can be pointed in the sense that the temperature-independent behavior of the FC magnetization below the blocking temperatures is conditioned by the magnitude of the activation energy, in terms of low temperature or low applied field, together with a condition of low degree of interactions between particles.

The magnetic moments provide a state of competing interactions, leading to a nonunique ground-state configuration. This competition between the magnetic moments is then attributed to the total magnetic moments of the particles. Since anisotropy and reversal mechanism are found to be critically determined by the spins of the surface atoms,[5,49] it is likely that dipolar interactions between surface atoms of adjacent particles impinge on the reorientation mechanism of the whole magnetic moment of the particle.[50] This scenario cannot be formally asserted here but may explain the observation of spin-canted and spin-glasslike behavior of surface spin in some magnetic particle systems. However, we observe in the low-temperature hysteresis loops of ANN-7 that the two branches converge at around $H=2500$ Oe. This fact, together with the practical superposition between the ZFC and the FC curves at $H=1000$ Oe (even at low temperatures), gives a signature of a re-entrant spin-glasslike behavior while lowering temperature and/or decreasing field, and thus it can be concluded that competing particle moments interact each other and that, at intermediate fields, superspin moment of a particle is sensitive to all the other moments by the field provided from the adjacent ferromagnetic particles.

Summarizing, it has been evidenced experimentally that a progressive increase in the interparticle interactions lead to a gradual modification of the spin state in magnetic granular

systems. When interactions appear, a first effect in the FC magnetothermal curves is the formation of a temperature-independent plateau below the maximum blocking temperature. It seems to be a first signature of spin freezing in which low temperatures, sufficiently low fields and weak interactions are involved. This first effect has been observed in ASD-25 that having iron particle with average size in the range of 0.9 nm shows a modified superparamagnetic behavior with spin freezing at low temperatures but with a $H^{3/2}$ dependence of the energy barriers and superparamagnetic features in the magnetization loops at temperatures above the blocking one.

Increasing interparticle interactions leads to the formation of a superspin-glass system, with a canonical $H^{2/3}$ dependence of the blocking temperatures, as shown in ANN-7 sample. Also, a frozen state of the superspins has been observed in the magnetic response for ac-susceptibility measurements, with a remarkable broadening of the energy distribution. The relatively large magnitude of the probing fields and the enhanced mean field provided by the increasing particle moments avoids the formation of a totally temperature-independent frozen spin state below the blocking temperatures in FC curves. Finally, decreasing interparticle distance leads to stronger interactions that yield a broader blocking distribution which results in a scarce dependence of ZFC magnetization with temperature and the appearance of superferromagnetic character, as observed in ANN-13 sample.

V. CONCLUSIONS

An exhaustive study of the magnetic interparticle interactions effects on the magnetic properties of granular Fe/Si_3N_4 systems is reported. Multilayered Fe/Si_3N_4 samples have been prepared by sequential sputtering under different conditions in order to tune their structural and magnetic properties. It has been observed that the annealed samples are conformed by discontinuous Fe layers when its nominal thickness approximates the average roughness, resulting in magnetic clusters embedded in a ceramic matrix. Moreover, a larger decoupling effect, accompanied by a shrink of the Fe particle size, was obtained in granular as-deposited samples. The variation in the metallic cluster size, d^{Fe}, intimately related to the nominal Fe layer thickness, t^{Fe}, of the primitive multilayer, leads to the modification of interparticle space and subsequently allows tuning the interparticle interactions of such system. In this way, samples with $t^{Fe}=1.3$ nm and 0.7 nm (namely, ANN-13 and ANN-7), present average particle sizes of $d^{Fe}\approx 3$ nm and $d^{Fe}\approx 1.3$ nm, respectively. On the other hand, as-deposited samples show an important presence of a nonmagnetic FeN phase, which for multilayers with magnetic granular behavior contribute decisively to reduce the Fe cluster dimensions, to separate the small magnetic Fe clusters and diminish their possible interparticle interaction (as in the case of the ASD-25 sample, with $t^{Fe}=2.5$ nm and an EXAFS-estimated average cluster size of $d^{Fe}=0.9$ nm.

Magnetic features confirm the granular behavior of these samples. An enhanced contribution of a superparamagnetic phase can be observed in their magnetization loops at room temperature. Remanence and coercivity show an abrupt decay with increasing temperature in samples with an average particle size of $d^{Fe}=0.9$ nm and $d^{Fe}=1.3$ nm, typical of magnetic particle systems, whereas samples with bigger sizes ($d^{Fe}=3$ nm) show ferromagnetic behavior, with a smaller dependence on temperature. ac-magnetization curves of $d^{Fe}\approx 1.3$ nm samples show a broad distribution of blocking temperatures, respect to the observed for $d^{Fe}\approx 0.9$ nm ones, as a result of both broadening of particle size distribution and increasing interparticle interactions. Also, differences in the frequency dependence of the peak temperature, T_{ac}^{max} where observed, showing a smaller variation in $d^{Fe}\approx 1.3$ nm samples. Both effects, broadening of the energy barrier distribution and smaller frequency dependence of T_{ac}^{max}, together with the differences of dispersion in the Cole-Cole plots, suggest that increasing interactions in the $d^{Fe}=1.3$ nm sample yield to the formation of an interacting particle system with superspin-glass behavior.

Magnetothermal ZFC-FC curves provide more information concerning to the blocking and reorientation processes of such interacting systems. A progressive modification in the magnetic behavior observed in the samples is explained in terms of their interparticle interactions. First, samples with very small particle size (ASD-25, $d^{Fe}\approx 0.9$ nm) presents a $T_B\sim H^{3/2}$ dependence, representative of noninteracting or very weakly interacting magnetic particle systems. However, an ordering temperature of $T_0\approx 10$ K and the presence of a scarce dependence of FC magnetization on temperature, resulting in a dip-and-plateau feature below T_B, point out to the existence of some weak dipolar interaction effects. In addition, increasing interactions lead to a critical modification of the magnetic behavior in such granular systems. Samples with slightly larger particle size (ANN-7, $d^{Fe}\approx 1.3$ nm) show an AT evolution ($T_B\sim H^{2/3}$) of the blocking temperature at intermediate fields ($100\leq H\leq 1000$ Oe), characteristic of superspin-glass behavior at temperatures below T_B. However, a decreasing magnetization with increasing temperature is observed in FC curves even at temperatures below T_B. This behavior can be explained in terms of stronger interactions between superspins oriented in the direction of the probing field. Finally, samples with $d^{Fe}\approx 3$ nm (ANN-13) present a superferromagnetic behavior due to a decrease in the interparticle space leading to stronger interactions.

In conclusion, an experimental evidence of the interparticle interaction effects in the magnetic properties of Fe/Si_3N_4 granular systems has been showed. Magnetization reversal and superspin reorientation in interacting particle systems are determined by the strength of the activation energy exerted to these systems, in terms of temperature, applied field, or interaction degree. In the first stage, weak interactions do not imply remarkable modifications respect to canonical superparamagnetic systems, exhibiting signatures of a frozen superspin state in FC magnetization curves at low temperatures, similar to interacting particle systems at very low probing fields. As particle coupling increases, the modified superparamagnetic behavior evolves into superspin-glass state, with a de Almeida-Thouless dependence of the blocking temperature with the applied field, and a remarkable broadening of the blocking distribution. Finally, stronger interactions tend to spread even more such blocking distribu-

tion and features of a superferromagnetic character becomes then displayed.

ACKNOWLEDGMENTS

This work has been supported by Spanish MICINN under Contracts No. MAT2009-08786, No. MAT2008-06517-C02-01, and No. CSD2009-00013 and by CAM under Contract No. S2009/MAT-1756. J.S.M. is grateful to MICINN for the financial support within the JdlC program. We acknowledge the European Synchrotron Radiation Facility for provision of x-ray beam. We would like to thank the SpLine CRG beamline staff for assistance during x-ray absorption experiments.

[1] J. Varalda, G. A. P. Ribeiro, M. Eddrief, M. Marangolo, J. M. George, V. H. Etgens, D. H. Mosca, and A. J. A. de Oliveira, J. Phys. D: Appl. Phys. **40**, 2421 (2007).
[2] F. Luis, J. M. Torres, L. M. García, J. Bartolomé, J. Stankiewicz, F. Petroff, F. Fettar, J. L. Maurice, and A. Vaurès, Phys. Rev. B **65**, 094409 (2002).
[3] A. García-García, A. Vovk, J. A. Pardo, P. Strichovanec, C. Magçen, E. Snoeck, P. A. Algarabel, J. M. de Teresa, L. Morellón, and M. R. Ibarra, J. Appl. Phys. **105**, 063909 (2009).
[4] X. Batlle and A. Labarta, J. Phys. D: Appl. Phys. **35**, R15 (2002).
[5] S. Rusponi, T. Cren, N. Weiss, M. Epple, P. Buluschek, L. Claude, and H. Brune, Nature Mater. **2**, 546 (2003).
[6] Y. Nahas, V. Repain, C. Chacon, Y. Girard, J. Lagoute, G. Rodary, J. Klein, S. Rousset, H. Bulou, and C. Goyhenex, Phys. Rev. Lett. **103**, 067202 (2009).
[7] A. Serrano, E. F. Pinel, A. Quesada, I. Lorite, M. Plaza, L. Pérez, F. Jiménez-Villacorta, J. de la Venta, M. S. Martín-González, J. L. Costa-Krämer, J. F. Fernandez, J. Llopis, and M. A. García, Phys. Rev. B **79**, 144405 (2009).
[8] E. Céspedes, Y. Huttel, L. Martínez, A. de Andrés, J. Chaboy, M. Vila, N. D. Telling, G. van der Laan, and C. Prieto, Appl. Phys. Lett. **93**, 252506 (2008).
[9] R. H. Kodama and A. E. Berkowitz, Phys. Rev. B **59**, 6321 (1999).
[10] J. R. L. de Almeida and D. J. Thouless, J. Phys. A **11**, 983 (1978).
[11] B. Martínez, X. Obradors, Ll. Balcells, A. Rouanet, and C. Monty, Phys. Rev. Lett. **80**, 181 (1998).
[12] H. Wang, T. Zhu, K. Zhao, W. N. Wang, C. S. Wang, Y. J. Wang, and W. S. Zhan, Phys. Rev. B **70**, 092409 (2004).
[13] J. M. Vargas, W. C. Nunes, L. M. Socolovsky, M. Knobel, and D. Zanchet, Phys. Rev. B **72**, 184428 (2005).
[14] T. Jonsson, P. Nordblad, and P. Svedlindh, Phys. Rev. B **57**, 497 (1998).
[15] J. L. Dormann, L. Bessais, and D. Fiorani, J. Phys. C **21**, 2015 (1988).
[16] W. Luo, S. R. Nagel, T. F. Rosenbaum, and R. E. Rosensweig, Phys. Rev. Lett. **67**, 2721 (1991).
[17] M. Suzuki, S. I. Fullem, I. S. Suzuki, L. Wang, and C. J. Zhong, Phys. Rev. B **79**, 024418 (2009).
[18] S. Sahoo, O. Petracic, Ch. Binek, W. Kleemann, J. B. Sousa, S. Cardoso, and P. P. Freitas, Phys. Rev. B **65**, 134406 (2002).
[19] S. Bedanta and W. Kleemann, J. Phys. D: Appl. Phys. **42**, 013001 (2009).
[20] P. Jönsson, M. F. Hansen, and P. Nordblad, Phys. Rev. B **61**, 1261 (2000).
[21] D. Parker, V. Dupuis, F. Ladieu, J.-P. Bouchaud, E. Dubois, R. Perzynski, and E. Vincent, Phys. Rev. B **77**, 104428 (2008).
[22] A. Kremenovic, B. Antic, V. Spasojevic, M. Vucinic-Vasic, Z. Jaglicic, J. Pirnat, and Z. Trontelj, J. Phys.: Condens. Matter **17**, 4285 (2005).
[23] F. Jiménez-Villacorta, E. Céspedes, M. Vila, A. Muñoz-Martín, G. R. Castro, and C. Prieto, J. Phys. D: Appl. Phys. **41**, 205009 (2008).
[24] R. Navamathavan, E. J. Yang, J. H. Lim, D. K. Hwang, J. Y. Oh, J. H. Yang, J. H. Jang, and S. J. Park, J. Electrochem. Soc. **153**, G385 (2006).
[25] Z. T. Kang, B. K. Wagner, J. Parrish, D. Schiff, and C. J. Summers, Nanotechnology **18**, 415709 (2007).
[26] K. Kato, D. Matsushita, K. Muraoka, and Y. Nakasaki, Phys. Rev. B **78**, 085321 (2008).
[27] M. Higashiwaki, Z. Chen, R. Chu, Y. Pei, S. Keller, U. K. Mishra, N. Hirose, T. Matsui, and T. Mimura, Appl. Phys. Lett. **94**, 053513 (2009).
[28] M. Vila, C. Prieto, A. Traverse, and R. Ramirez, J. Appl. Phys. **98**, 113507 (2005).
[29] D. Zanghi, A. Traverse, S. Gautrot, and O. Kaïtasov, J. Mater. Res. **16**, 512 (2001).
[30] N. D. Telling, S. J. Guilfoyle, D. R. Lovett, C. C. Tang, M. D. Crapper, and M. Petty, J. Phys. D: Appl. Phys. **31**, 472 (1998).
[31] Y. Kong, J. Phys.: Condens. Matter **12**, 4161 (2000).
[32] I. Arcon, A. Tuel, A. Kodre, G. Martin, and A. Barbier, J. Synchrotron Radiat. **8**, 575 (2001).
[33] F. Jiménez-Villacorta, A. Muñoz-Martín, and C. Prieto, J. Appl. Phys. **96**, 6224 (2004).
[34] J. B. Sousa, J. A. M. Santos, R. F. A. Silva, J. M. Teixeira, J. Ventura, J. P. Araújo, P. P. Freitas, S. Cardoso, Yu. G. Pogorelov, G. N. Kakazei, and E. Snoeck, J. Appl. Phys. **96**, 3861 (2004).
[35] S. Morup, M. B. Madsen, J. Franck, J. Villadsen, and C. J. W. Koch, J. Magn. Magn. Mater. **40**, 163 (1983).
[36] S. Bedanta, J. Rhensius, W. Kleeman, P. Parashar, S. Cardoso, and P. P. Freitas, J. Appl. Phys. **105**, 07C306 (2009).
[37] W. Kleemann, O. Petracic, Ch. Binek, G. N. Kakazei, Y. G. Pogorelov, J. B. Sousa, S. Cardoso, and P. P. Freitas, Phys. Rev. B **63**, 134423 (2001).
[38] S. Bedanta, T. Eimüller, W. Kleemann, J. Rhensius, F. Stromberg, E. Amaladass, S. Cardoso, and P. P. Freitas, Phys. Rev. Lett. **98**, 176601 (2007).
[39] W. C. Nunes, L. M. Socolovsky, J. C. Denardin, F. Cebollada, A. L. Brandl, and M. Knobel, Phys. Rev. B **72**, 212413 (2005).
[40] S. K. Sharma, R. Kumar, S. Kumar, M. Knobel, C. T. Meneses, V. V. S. Kumar, V. R. Reddy, M. Singh, and C. G. Lee, J. Phys.: Condens. Matter **20**, 235214 (2008).
[41] S. Shtrikman and E. P. Wohlfarth, Phys. Lett. A **85**, 467 (1981).
[42] B. Idzikowski, U. K. Robler, D. Eckert, K. Nenkov, K. Dorr, and K. H. Muller, Europhys. Lett. **45**, 714 (1999).
[43] J. L. Tholence, Physica B **108**, 1287 (1981).

[44] K. S. Cole and R. H. Cole, J. Chem. Phys. **9**, 341 (1941).
[45] R. H. Victora, Phys. Rev. Lett. **63**, 457 (1989).
[46] I. Prigogine, S. A. Rice, J. L. Dormann, D. Fiorani, and E. Tronc, Adv. Chem. Phys. **98**, 283 (1997).
[47] R. W. Chantrell, N. Walmsley, J. Gore, and M. Maylin, Phys. Rev. B **63**, 024410 (2000).
[48] O. Petracic, X. Chen, S. Bedanta, W. Kleemann, S. Sahoo, S. Cardoso, and P. Freitas, J. Magn. Magn. Mater. **300**, 192 (2006).
[49] C. L. Chien, J. Appl. Phys. **69**, 5267 (1991).
[50] E. Winkler, R. D. Zysler, M. Vasquez Mansilla, D. Fiorani, D. Rinaldi, M. Vasilakaki, and K. N. Trohidou, Nanotechnology **19**, 185702 (2008).